3 1176 00105 1326

RESEARCH MEMORANDUM

INVESTIGATION OF THE LATERAL STABILITY CHARACTERISTICS

OF THE DOUGLAS X-3 CONFIGURATION AT MACH NUMBERS

FROM 0.6 TO 1.1 BY MEANS OF A

ROCKET-PROPELLED MODEL

By Jesse L. Mitchell and Robert F. Peck

Langley Aeronautical Laboratory
Langley Field, Va.

NATIONAL ADVISORY COMMITTEE
FOR AERONAUTICS
WASHINGTON
February 15, 1955

NATIONAL ADVISORY COMMITTEE FOR AERONAUTICS

RESEARCH MEMORANDUM

INVESTIGATION OF THE LATERAL STABILITY CHARACTERISTICS

OF THE DOUGLAS X-3 CONFIGURATION AT MACH NUMBERS

FROM 0.6 TO 1.1 BY MEANS OF A

ROCKET-PROPELLED MODEL

By Jesse L. Mitchell and Robert F. Peck

SUMMARY

A rocket-propelled model of the Douglas X-3 airplane has been flown to investigate the lateral stability characteristics of this configuration at approximately zero angle of attack and to evaluate briefly the test and analysis technique.

Time histories of the lateral motion following pulse-type disturbances indicate that the model was, in general, dynamically stable throughout the Mach number range from 0.6 to 1.1. However, in the region where the oscillations were allowed to persist without further disturbance, an undamped oscillation of 1° sideslip remained after an initially damped oscillation. Rather abrupt changes in lateral trim and in the characteristics of the Dutch-roll oscillation occurred in the Mach number region 0.9 to 1.07.

A vector analysis of the Dutch-roll oscillation was used and found to give useful approximations for some of the lateral stability derivatives. This analysis indicates that the effective dihedral $-C_{l_\beta}$ and damping in roll C_{l_p} increase while the static directional stability C_{n_β} and the damping in yaw $C_{n_r} - C_{n_{\dot\beta}}$ decrease appreciably as the Mach number is increased from 0.95 to 1.07. The variation of lateral force with sideslip C_{Y_β} remains about constant throughout the Mach number region of the test.

Comparisons between the rocket-propelled-model test data and results from other rocket-propelled-model and wind-tunnel data were made when possible. The results of the present test are, in general, in good agreement with the other results.

INTRODUCTION

Rocket-propelled models have been used extensively by the Langley Pilotless Aircraft Research Division to investigate the longitudinal stability and lift characteristics of airplane configurations such as the Douglas X-3 (ref. 1). As a by-product of these investigations, a limited amount of information on lateral stability has also been obtained (ref. 2). Recently a model was flown specifically to investigate the lateral stability characteristics of the X-3 airplane and to make some evaluation of the test technique. The data obtained from the test are presented in this report.

The test technique was similar to that used to investigate longitudinal stability characteristics, in that it involved measurements of the transient motion. In the present test a transient motion in the lateral mode was induced by the periodic firing of small pulse rockets mounted in the nose of the model.

The characteristics of the Dutch-roll mode of lateral motion were obtained in the Mach number range from 0.6 to 1.1 at Reynolds numbers from 4×10^6 to 10×10^6. An analysis of the data by use of the concept of rotating vectors for the various components of the motion (refs. 3 to 6) gave values for some of the lateral stability derivatives.

SYMBOLS

All forces and moments unless otherwise noted are referred to a body axis system which is defined in figure 1.

C_X longitudinal-force coefficient, X/qS

C_Y lateral-force coefficient, Y/qS

C_Z normal-force coefficient, Z/qS

C_l rolling-moment coefficient, L/qSb

C_n yawing-moment coefficient, N/qSb

C_L lift coefficient, $-C_Z \cos \alpha + C_X \sin \alpha$

at/g lateral load factor as indicated by accelerometer at center of gravity; aerodynamic lateral force is $(at/g)W$

α angle of attack, radians and deg

β angle of sideslip, radians and deg

θ angle of pitch, radians and deg

ψ angle of yaw, radians and deg

φ angle of roll, radians and deg

$\dot{\beta}$ rate of change of angle of sideslip with time, radians/sec

$\dot{\psi},r$ yawing angular velocity, radians/sec

$\dot{\varphi},p$ rolling angular velocity, radians/sec

$\ddot{\psi}$ rate of change of yawing angular velocity with time, radians/sec/sec

$\ddot{\varphi}$ rate of change of rolling angular velocity with time, radians/sec/sec

P period of lateral oscillation, sec

ω frequency of lateral oscillation, radians/sec

$t_{\dot{\varphi}}$ time lag between p and $-\beta$ in lateral oscillation, sec

$\Omega_{\dot{\varphi}}$ phase angle between p and β in lateral oscillation,

$$\pi - 2\pi \frac{t_{\dot{\varphi}}}{P}, \text{ radians}$$

Ω_{C_Y} phase angle between C_Y and β in lateral oscillation, radians

$T_{1/2}$ time for lateral oscillation to damp to one-half amplitude, sec

a damping factor, $\dfrac{-0.693}{T_{1/2}}$, 1/sec

$\bar{c}$ mean aerodynamic chord

V velocity, ft/sec

M Mach number

R   Reynolds number

q   dynamic pressure, lb/ft^2

p/p_0 ratio of atmospheric static pressure p to standard sea level pressure p_0 where $p_0 = 2116$ lb/ft^2

W   weight of model, lb

m   mass of model, slugs

ϵ inclination of principal axis, positive as shown in fig. 1

I_X moment of inertia about X-axis, $slug\text{-}ft^2$

I_Z moment of inertia about Z-axis, $slug\text{-}ft^2$

I_{XZ} product of inertia, $\frac{1}{2}(I_Z - I_X)\tan 2\epsilon$, $slug\text{-}ft^2$

S   wing area, ft^2

b   wing span, ft

l vertical tail length, distance from center of gravity to center of pressure of vertical tail, ft

A   aspect ratio

λ taper ratio, $\frac{\text{Tip chord}}{\text{Root chord}}$

The amplitude ratio of the indicated quantities in the lateral oscillation is indicated in the following manner: $\left|\frac{C_Y}{\beta}\right|$, $\left|\frac{\dot{\beta}}{\beta}\right|$, $\left|\frac{\dot{\phi}}{\beta}\right|$. The lateral stability derivatives are indicated, for example, by $C_{Y_\beta} = \frac{\partial C_Y}{\partial \beta}$; $C_{Y_{\dot\beta}} = \frac{\partial C_Y}{\frac{\partial \dot\beta b}{2V}}$.

MODEL AND TESTS

Model

The Douglas X-3 configuration tested was the same with the exception of the tail boom as that used in the longitudinal tests of reference 1. The boom was built up along the forward portion with fiberglass so as to correspond more closely to the boom of the final airplane configuration. A sketch of the 0.16-scale model is shown in figure 2.

The model was of metal construction with the exception of the previously mentioned portion of the boom. The body was made of magnesium castings and duralumin sheet, and the wing and tail surfaces were solid duralumin. The wing and vertical tail were 4.5 percent thick and the horizontal tail was 5.0 percent thick. The deflection of the horizontal tail was -1.0 degree. All surfaces had a modified hexagonal airfoil section.

The inlets were connected to constant-diameter ducts designed for choked flow at the exits with a mass-flow ratio of about 0.8.

The weight of the model was 154 pounds; and the center of gravity was 1.0 percent ahead of the leading edge of the mean aerodynamic chord of the wing. The moments of inertia about X- and Z-axes (fig. 2) were 1.18 and 18.2 slug-ft^2, respectively. The principal axis was inclined 4.8°, nose down, (see fig. 2), which gave a product of inertia of 1.44 slug-ft^2.

Test

The model was boosted to a maximum Mach number of about 1.2 by means of an ABL Deacon rocket motor (fig. 3), from which it separated at rocket burnout. Six pulse rockets mounted in the nose of the model, each rocket with a total impulse of 6 pound-seconds and a burning time of 0.08 second, were fired periodically during the coasting part of the flight. Time histories of the resulting motion of the model were obtained from an NACA telemetering and instrumentation system. The following continuous telemeter information obtained were normal, longitudinal, and transverse acceleration near the center of gravity, transverse acceleration at a point in the nose, angle of sideslip, angle of attack, rate of roll, and free-stream total pressure. The flight path of the model was obtained from an NACA modified SCR 584 tracking radar, and a radiosonde was used to check the free-stream conditions at the model during the flight. In addition, the CW Doppler velocimeter furnished a check on the velocity.

Variations in the static pressure ratio and Reynolds number with Mach number are shown in figure 4.

ANALYSIS

Vector Method

A vector-analysis procedure similar to those discussed in references 3 to 6 and to some unpublished work done at the Langley Laboratory during the summer of 1952 by E. E. Larrabee was used to obtain the lateral stability derivatives: C_{l_β}, C_{l_p}, C_{n_β}, and $C_{n_r} - C_{n_{\dot\beta}}$.

The information available for this analysis at any time during the flight of the model was geometry, mass, moments of inertia, product of inertia, velocity, dynamic pressure, Mach number, aerodynamic lateral-force coefficient, angle of sideslip, angle of attack, rate of roll, and angular acceleration in yaw.

From the above information, the essential features of the oscillatory or Dutch-roll part of the lateral response to the pulse disturbances were obtained as a function of Mach number. These characteristics of the oscillation were the period, damping factor, time lag between sideslip and lateral force, time lag between sideslip and roll rate and the ratios of the envelopes of the oscillations of side force, roll rate, and angular acceleration in yaw to sideslip angle.

These measured characteristics of the lateral response were then assumed to be governed by the following equations of motion taken about the body axis system shown in figure 1, since all flight instrumentation was alined with these axes:

lateral force:

$$\frac{mV}{qS}(\dot\beta + \dot\psi - \alpha\dot\varphi) = C_{Y_\beta}\beta + C_{Y_{\dot\beta}}\frac{\dot\beta b}{2V} + C_{Y_r}\frac{rb}{2V} + C_{Y_p}\frac{pb}{2V} + \frac{W}{qS}(\varphi\cos\theta + \psi\sin\theta)$$

rolling moment:

$$\frac{I_X}{qSb}\ddot\varphi - \frac{I_{XZ}}{qSb}\ddot\psi = C_{l_\beta}\beta + C_{l_{\dot\beta}}\frac{\dot\beta b}{2V} + C_{l_r}\frac{rb}{2V} + C_{l_p}\frac{pb}{2V}$$

yawing moment:

$$\frac{I_Z}{qSb}\ddot\psi - \frac{I_{XZ}}{qSb}\ddot\varphi = C_{n_\beta}\beta + C_{n_{\dot\beta}}\frac{\dot\beta b}{2V} + C_{n_r}\frac{rb}{2V} + C_{n_p}\frac{pb}{2V}$$

On the basis of preliminary calculations and by consideration of the data available for analysis, it was found that these equations could be somewhat simplified for the present test:

lateral force:

$$\frac{mV}{qS}(\dot{\beta} + \dot{\psi} - \alpha\dot{\phi}) = \frac{at}{g}\frac{W}{qS} = C_Y$$

rolling moment:

$$\frac{I_X}{qSb}\ddot{\phi} - \frac{I_{XZ}}{qSb}\ddot{\psi} = C_{l_\beta}\beta + C_{l_p}\frac{\dot{\phi}b}{2V} + C_{l_r}\frac{\dot{\psi}b}{2V}$$

yawing moment:

$$\frac{I_Z}{qSb}\ddot{\psi} - \frac{I_{XZ}}{qSb}\ddot{\phi} = C_{n_\beta}\beta + C_{n_p}\frac{\dot{\phi}b}{2V} + \left(C_{n_r} - C_{n_{\dot{\beta}}}\right)\frac{\dot{\psi}b}{2V}$$

The lateral-force equation neglects the lateral force due to gravity. It includes all the aerodynamic forces since they were measured by the transverse accelerometer. The rolling-moment equation assumes $C_{l_{\dot{\beta}}} = 0$. The combination derivative $C_{n_r} - C_{n_{\dot{\beta}}}$ as now included in the yawing-moment equation tacitly assumes $\dot{\beta} = -\dot{\psi}$ for this equation only. The equations in this simplified form are believed to be satisfactory for the present test conditions. Other test conditions will require an examination of the more general equations to determine whether similar simplications are applicable.

The measured oscillatory motions resulting from the yaw disturbance were then assumed to be given by:

$$\beta = \beta_o e^{at}\cos \omega t$$

$$C_Y = \left|\frac{C_Y}{\beta}\right|\beta_o e^{at}\cos\left(\omega t + \Omega_{C_Y}\right)$$

$$\dot{\phi} = \left|\frac{\dot{\phi}}{\beta}\right|\beta_o e^{at}\cos\left(\omega t + \Omega_{\dot{\phi}}\right)$$

The derivatives and integrals of these quantities are known as well, such as,

$$\dot{\beta} = \sqrt{a^2 + \omega^2}\,\beta_0 e^{at} \cos\left(\omega t + \tan^{-1}\frac{\omega}{a}\right)$$

With the above assumptions and β as unit amplitude, the quantities β, C_Y, $\dot{\phi}$, $\dot{\beta}$, and $\ddot{\phi}$ may be represented as vectors rotating with frequency ω, and with amplitudes and phases as shown in the following table:

	β	C_Y	$\dot{\phi}$	$\dot{\beta}$	$\ddot{\phi}$
Amplitude	1	$\left\|\dfrac{C_Y}{\beta}\right\|$	$\left\|\dfrac{\dot{\phi}}{\beta}\right\|$	$\sqrt{a^2 + \omega^2}$	$\sqrt{a^2 + \omega^2}\left\|\dfrac{\dot{\phi}}{\beta}\right\|$
Phase	0	Ω_{C_Y}	$\Omega_{\dot{\phi}}$	$\tan^{-1}\dfrac{\omega}{a}$	$\Omega_{\dot{\phi}} + \tan^{-1}\dfrac{\omega}{a}$

The vector solution of the equations of motion is illustrated in figure 5. The lateral-force equation is solved first for the yawing-velocity vector. This equation also gives the yawing acceleration vector. A check on the amplitude ratio of the yawing acceleration $\left|\dfrac{\ddot{\psi}}{\beta}\right|$ obtained from this solution is furnished by the yawing acceleration measured from the two transverse accelerometers.

After the yawing velocity and acceleration vectors are obtained from the lateral force-equation, either the rolling-moment or yawing-moment equation may be solved. For the moment equations, the inertia vectors are known; thus, three vectors remain which are known only in direction and are proportional to the derivatives C_{l_r}, C_{l_p}, and C_{l_β} for the rolling moment and to the derivatives C_{n_β}, C_{n_p}, and $C_{n_r} - C_{n_{\dot{\beta}}}$ for the yawing moment. The general procedure at this point is to estimate the amplitude of the smallest vector so that the other two may be obtained by closing the vector polygon. For the present tests the C_{l_r} and C_{n_p} vectors were estimated, and the values of C_{l_p}, C_{l_β}, C_{n_β}, and $C_{n_r} - C_{n_{\dot{\beta}}}$ were obtained by closing the polygons.

It can be seen from the vector diagram that the solutions for the various derivatives are linear functions of the assumed derivatives. Thus, in practice it is easy to obtain the value of C_{l_p}, for example,

for any number of assumptions for C_{l_r}.

Quasi-Static Method

In addition to the vector analysis for derivatives, the lateral-force, yawing-moment, and rolling-moment coefficients were obtained as functions of sideslip angle as follows:

$$C_Y(\beta) = \frac{at}{g}\frac{W}{qS}$$

$$C_n(\beta) = \frac{I_Z}{qSb}\ddot{\psi} - \frac{I_{XZ}}{qSb}\ddot{\phi} - \left(C_{n_r} - C_{n_{\dot\beta}}\right)\frac{\dot\psi b}{2V} - C_{n_p}\frac{\dot\phi b}{2V}$$

$$C_l(\beta) = \frac{I_X}{qSb}\ddot{\phi} - \frac{I_{XZ}}{qSb}\ddot{\psi} - C_{l_r}\frac{\dot\psi b}{2V} - C_{l_p}\frac{\dot\phi b}{2V}$$

The side force due to sideslip angle $C_Y(\beta)$ was taken equal to the total measured side force since the measured side force was essentially 180° out of phase with the sideslip angle. This is tantamount

to the assumption $C_{Y_p}\frac{\dot\phi b}{2V} + C_{Y_r}\frac{\dot\psi b}{2V} + C_{Y_{\dot\beta}}\frac{\dot\beta b}{2V} = 0$. The yawing and rolling

moments due to sideslip angle, $C_n(\beta)$ and $C_l(\beta)$, respectively, were assumed to be given by the total measured moments corrected for the moments due to yawing and rolling velocities. The yawing angular acceleration $\ddot{\psi}$ was obtained from two accelerometers and the rolling angular acceleration $\ddot{\phi}$ was obtained from differentiation of the roll rate. The values of the derivatives C_{n_p} and C_{l_r} were estimated and $C_{n_r} - C_{n_{\dot\beta}}$, C_{l_p}, and $\dot\psi$ were obtained from the vector solution.

A body-axis system was used for the sake of convenience and all flight instrumentation was alined with the system. The derivative obtained may be converted to a stability-axis system, but, in this particular case, differences would be small since α is always near zero.

ACCURACY AND CORRECTIONS

Accuracy

The estimated probable errors in the basic measurements are indicated in table I. The derivatives C_{Y_β}, C_{n_β}, C_{l_β}, C_{l_p}, and $C_{n_r} - C_{n_{\dot\beta}}$ are functions of some or all of the quantities.

The incremental error in C_{l_β}, for instance, due to the error in I_X was taken as

$$\left(\Delta C_{l_\beta}\right)_{I_X} = \frac{\partial C_{l_\beta}}{\partial I_X} \Delta I_X$$

where the partial derivative of C_{l_β} with respect to I_X was obtained from an analytical solution of the vector diagram. The probable error in C_{l_β} due to all the probable errors in table I was taken as in reference 7 to be

$$\left(\Delta C_{l_\beta}\right)_{\text{probable}} = \sqrt{\left[\left(\Delta C_{l_\beta}\right)_{I_X}\right]^2 + \left[\left(\Delta C_{l_\beta}\right)_{I_Z}\right]^2 + \dots}$$

Table II gives the results of this error analysis. The increments due to errors in each of the basic measured quantities are given to illustrate the relative importance of accuracy of each measurement. The given probable error $\sqrt{\Sigma(\text{increments})^2}$ shows accuracies of 3 to 10 percent for C_{Y_β}, 6 to 13 percent for C_{n_β} and C_{l_β}, 12 to 17 percent for C_{l_p}, and 14 to 26 percent for $C_{n_r} - C_{n_{\dot\beta}}$.

As mentioned in the analysis, it was necessary to make estimates of C_{l_r} and C_{n_p} in order to complete the rolling and yawing-moment diagrams. The effects on each of the derivatives of changing C_{l_r} and C_{n_p} by 0.1 are also shown in table II. Changing C_{l_r} and C_{n_p} by 0.1 had small effect on C_{n_β} and C_{l_β} but had very noticeable effects on C_{l_p} and $C_{n_r} - C_{n_{\dot\beta}}$ (same order as probable accuracies).

   The accuracies presented were calculated for the vector analysis
but are also representative of the absolute accuracy of derivatives
obtained by other methods. It is believed that the data presented in
this report provide a good indication of how the lateral stability deriv-
atives for this configuration vary with Mach number and sideslip angles.
Comparisons between methods and tests made throughout the report indicate
that the absolute accuracy of these derivatives is at least as good as
or better than that indicated by information in table II.

                               Corrections

   The angles of attack and sideslip as measured ahead of the nose of
the model were corrected for flight-path-curvature effects to the center
of gravity by the method given in reference 8.

   None of the accelerometers could be mounted exactly at the center
of gravity, but model motions (angular accelerations and velocities) were
measured sufficiently well to enable corrections where necessary.

   The model response frequency was always less than 4 percent of any
instrument natural frequency, and no frequency-response corrections were
necessary with the exception of phase-angle data from the roll rate gyro.
Frequency-response corrections to the phase angle between $\dot\phi$ and β
were from 1° to 2°.

                          RESULTS AND DISCUSSION

                            Time Histories

   The essential characteristics of the lateral motions following the
pulse-rocket disturbances are shown in the time histories of Mach number,
angle of attack, angle of sideslip, and rate of roll, in figure 6. In
general, the appearance of the oscillations in sideslip angle and roll
rate is that of a damped sinusoid. However, the oscillation beginning
at about 9.2 seconds is damped only until the amplitude of the angle of
sideslip reaches about 1°. At this point the oscillation persists at
an essentially constant amplitude. Previous to this time the spacing
of the pulse disturbances was so close that it is not known whether such
damping characteristics were present. An examination of the telemeter
record after 17 seconds shows a similar effect.

   Some of the pulse rockets caused an appreciable rolling-moment
disturbance as can be seen by an examination of the roll rate response
at 6 and 7 seconds. However, the disturbance was still so small when

compared with the oscillatory response that no reliable quantitative measurements were obtained of the roll-subsidence mode of the lateral response.

The regions of the time history where cross plots and vector diagram were used to analyze the data are indicated on the time history. The change in Mach number and in angle of attack in these regions is, in general, believed to be small enough so as to have a minor effect on the lateral motions. In particular, the effects of inertia coupling (see ref. 9) due to combined longitudinal and lateral motion have been checked. This check indicated that the inertia coupling effects were small.

Lateral Trim Characteristics

The trim characteristics as a function of Mach number are presented in figure 7. A lateral trim change is indicated in the Mach number region between 0.9 and 1.05. This occurs along with the characteristic longitudinal trim change also presented in figure 7. The variations of sideslip angle β and lateral-force coefficient C_Y with Mach number are consistent although the absolute magnitudes appear to be inconsistent since the model was supposedly symmetrical. These and subsequent data are all presented as measured, however, and no arbitrary corrections have been applied to satisfy considerations of symmetry.

General Characteristics of the Lateral Oscillation

The characteristics of the Dutch-rolling oscillation are presented in figure 8. Generally the most notable variations with Mach number are in the region of the lateral trim change where M has values from 0.9 to 1.05.

Lateral Stability Derivatives

Quasi-static analysis.- The variation of lateral-force coefficient, yawing-moment coefficient, and rolling-moment coefficient with angle of sideslip and Mach number are shown in figure 9. These coefficients were obtained as functions of β as indicated in the analysis.

The straight lines through the data points for C_Y, C_n, and C_l are drawn with the slope used in or obtained from the vector diagrams. Wind-tunnel data from reference 10 for a Mach number of 0.9 are also shown. The wind-tunnel data indicate a marked reduction in slope at small angles of sideslip, but the slope at moderate angles is about the same as that of the present test. The linear variation from the vector

solution is in general a good representation of the rocket-propelled-model data; however, a close examination indicates some small nonlinear tendency similar to that of the wind-tunnel results. The fact that the rocket-propelled-model data indicate a more nearly linear variation of force and moment coefficients with angle of sideslip at a Mach number of 0.9 than do the data of reference 10 is most likely due to a Reynolds number effect on the sharp nose airfoil section. The Reynolds numbers of the wind-tunnel and rocket-propelled-model tests were 2.3×10^6 and 7.4×10^6, respectively.

Vector analysis.- Although the validity of a linearized solution may be questioned in certain regions of the time history where the oscillations are not well defined damped cosine curves, it is believed that the results obtained from such an analysis furnish useful approximations. The essential validity is indicated, for instance, by the rather good agreement between the values of the amplitude ratio $\left| \dfrac{\ddot{\psi}}{\beta} \right|$ as obtained from the vector solution as compared with the amplitude ratio obtained from the measured time history of $\ddot{\psi}$ (fig. 8(c)). Also, the fact that the yawing-moment and rolling-moment coefficients of figure 9 agree reasonably well with the linear variation given by the vector solutions indicates at least the essential validity of the solution as far as the determination of the static derivatives C_{n_β} and C_{l_β} are concerned.

As was discussed in the analysis, it was necessary to assume values of C_{l_r} and C_{n_p}. The estimated value for C_{l_r} was about 0.2 and for C_{n_p} the value was about 0.1 throughout the Mach number range of the test. In order to indicate the sensitivity of the various derivatives to these assumptions, the increment changes in the derivatives for a change of 0.1 in C_{l_r} and C_{n_p} are given in table II.

It can be seen that the static derivatives C_{n_β} and C_{l_β} are relatively insensitive to the assumed values of C_{n_p} and C_{l_r}. The damping derivatives C_{l_p} and $C_{n_r} - C_{n_{\dot\beta}}$ are relatively more sensitive to the assumptions. A change in the estimated value of C_{l_r} from 0.2 to 0.1 makes a maximum change of about 0.04 in C_{l_p}. A change of from 0.1 to 0.2 in the estimated value of C_{n_p} makes a maximum change of about 0.4 in the value of $C_{n_r} - C_{n_{\dot\beta}}$.

The fact that the static derivatives C_{l_β} and C_{n_β} are relatively insensitive to the assumed values of the cross derivatives C_{l_r} and C_{n_p} indicates that the vector technique applied to data on the Dutch-roll oscillation alone may be sufficient to determine usable values of these derivatives. The relative sensitivity of the damping derivatives C_{l_p} and $C_{n_r} - C_{n_{\dot\beta}}$ to the assumptions perhaps indicates the need for further refinements and additions to the test technique. For instance, if the damping-in-roll subsidence could also be determined, then the characteristic equation of lateral motion along with the relations of the roots of the equation to its coefficients could be used as an additional aid to the determination of the derivatives, especially the damping-in-roll derivative C_{l_p}.

It is of interest to note also that conditions favorable to the determination of these damping derivatives from the Dutch-roll oscillation might be obtained by judicious choice of test conditions (moments of inertia, dynamic pressure, etc.) so that the assumed quantities would have a much smaller effect on the result.

The results of the vector analysis for the static derivatives C_{l_β} and C_{n_β} are shown in figure 10 along with C_{Y_β} as determined from the cross plot of figure 9(a).

Shown for comparison are wind-tunnel data at Mach numbers of 0.9 and 1.4 from reference 10. The tunnel values at a Mach number of 0.9 are the average of the slopes at $\pm 3^\circ$ sideslip (see fig. 8), whereas the values at a Mach number of 1.4 are those at zero angle of sideslip. Also shown in figure 10 is C_{n_β} as it was obtained from the analysis with a single degree of freedom. This analysis, which neglects the product-of-inertia term, is seen to give consistently low values for the present test although the trend with Mach number is the same as that indicated by the more complete vector solution.

The results of the vector analysis for the damping derivatives C_{l_p} and $C_{n_r} - C_{n_{\dot\beta}}$ are given in figure 11.

Theoretical estimates of C_{l_p} from references 11 and 12 are shown in figure 11 along with experimental data for a wing with an aspect ratio of 3 from the wind-tunnel test of reference 13 and for a wing with an aspect ratio of 4 from the rocket-propelled-model test of reference 14. The data from the present test are in fair to good agreement with both theory and the other experimental data.

The contribution of the vertical tail to $C_{n_r} - C_{n_{\dot\beta}}$ was estimated and is shown in figure 11. This estimate was made by using the data at a Mach number of 1.4 (ref. 9) to obtain the ratio of C_{Y_β} of the vertical tail to C_{Y_β} of the complete configuration. In general, the damping derivative is more negative than this estimate, and it appears that appreciable contributions to $C_{n_r} - C_{n_{\dot\beta}}$ come from the boom, fuselage, wing, and possibly interference effects such as sidewash. The low values of $C_{n_r} - C_{n_{\dot\beta}}$ shown by flagged symbols were obtained from the relatively low amplitude, undamped portion (between 11.2 and 13.4 seconds) of the oscillation which began at 9.3 seconds (see fig. 6). In the vector analysis it was assumed that all variables other than $C_{n_r} - C_{n_{\dot\beta}}$ were the same as for the higher amplitude portion of this oscillation. This assumption results in the indication that the lack of damping during this part of the flight resulted from a low value of $C_{n_r} - C_{n_{\dot\beta}}$, that is, a nonlinear effect of β amplitude on $C_{n_r} - C_{n_{\dot\beta}}$. This may not be the case, however. For instance, if C_{n_p} at these conditions were -0.1 instead of the assumed value of 0.1, the values of $C_{n_r} - C_{n_{\dot\beta}}$ would be on approximately the same level as the other points.

The lateral-force derivative C_{Y_β} is the only derivative which shows no marked variation with Mach number. The variations of the other derivatives with Mach number are in general most noticeable in the region from 0.95 to 1.07. In this region the effective dihedral $-C_{l_\beta}$ increases about 50 percent; the damping in roll C_{l_p} increases about 40 percent; and the damping in yaw $C_{n_r} - C_{n_{\dot\beta}}$ decreases by 20 to 30 percent. As can be seen in figure 7, these changes were reflected in the general characteristics of the Dutch-roll motion. It should also be pointed out that the angle-of-attack changes in the Mach number region from 0.95 to 1.07. Therefore, a small part of the apparent effect of Mach number indicated may be due to the change in angle of attack.

CONCLUDING REMARKS

The results from the flight of a rocket-propelled model of the Douglas X-3 airplane in which measurements of the transient lateral oscillation were made indicate the following conclusions:

The lateral characteristics of the model were such that it was, in general, dynamically stable throughout the Mach number range from 0.6 to 1.1. However, in the Mach number regions where the oscillation was allowed to persist long enough (only data below a Mach number of about 0.75), an essentially undamped oscillation of 1° sideslip persisted after an initially damped oscillation. The Mach number region from 0.90 to 1.1 was characterized by a lateral trim change as well as other abrupt changes in the characteristics of the Dutch-roll oscillation.

A vectorial concept of the various components of the Dutch-roll lateral motion furnished a useful basis for the analysis of the data. The results obtained from the vector analysis indicate that with increase in Mach number in the Mach number region from 0.95 to 1.07, the effective dihedral $-C_{l_\beta}$ and the damping in roll C_{l_p} increased while the static directional stability C_{n_β} and damping in yaw $C_{n_r} - C_{n_{\dot\beta}}$ decreased. At a Mach number of 0.9 the rocket-propelled-model data at a Reynolds number of 7.4×10^6 and the wind-tunnel data at a Reynolds number of 2.29×10^6 showed the same values of C_{Y_β}, C_{l_β}, and C_{n_β} at moderate angles of sideslip. The rocket-propelled-model data at the higher Reynolds numbers did not indicate the same reductions in C_{Y_β}, C_{l_β}, and C_{n_β} at the small angles of sideslip as was shown by the wind-tunnel data.

Langley Aeronautical Laboratory,
    National Advisory Committee for Aeronautics,
        Langley Field, Va., December 9, 1954.

REFERENCES

1. Peck, Robert F., and Hollinger, James A.: A Rocket-Model Investigation of the Longitudinal Stability, Lift, and Drag Characteristics of the Douglas X-3 Configuration With Horizontal Tail of Aspect Ratio 4.33. NACA RM L53F19a, 1953.

2. Purser, Paul E., and Mitchell, Jesse L.: Miscellaneous Directional-Stability Data for Several Airplane-Like Configurations From Rocket-Model Tests at Transonic Speeds. NACA RM L52E06b, 1952.

3. Mueller, R. K.: The Graphical Solution of Stability Problems. Jour. Aero. Sci., vol. 4, no. 8, June 1937, pp. 324-331.

4. Breuhaus, W. O.: Resumé of the Time Vector Method as a Means for Analyzing Aircraft Stability Problems. WADC Tech. Rep. 52-299 (Contract No. AF 33(038)-20659 RDO No 461-1-2), Wright Air Dev. Center, U. S. Air Force, Nov. 1952.

5. Larrabee, E. E.: Application of the Time Vector Method to the Analysis of Flight Test Lateral Oscillation Data. FRM No. 189, Cornell Aero. Lab., Inc., Sept. 9, 1953.

6. Sternfield, L.: A Vector Method Approach to the Analysis of the Dynamic Lateral Stability of Aircraft. Jour. Aero. Sci., vol. 21, no. 4, Apr. 1954, pp. 251-256.

7. Eshbach, Ovid W., ed.: Handbook of Engineering Fundamentals. John Wiley & Sons, Inc., 1936.

8. Ikard, Wallace L.: An Air-Flow-Direction Pickup Suitable for Telemetering Use on Pilotless Aircraft. NACA RM L53K16, 1954.

9. Parks, James H.: Experimental Evidence of Sustained Coupled Longitudinal and Lateral Oscillations From a Rocket-Propelled Model of a 35° Swept Wing Airplane Configuration. NACA RM L54D15, 1954.

10. Olson, Robert N., and Chubb, Robert S.: Wind-Tunnel Tests of a 1/12-Scale Model of the X-3 Airplane at Subsonic and Supersonic Speeds. NACA RM A51F12, 1951.

11. DeYoung, John: Theoretical Antisymmetric Span Loading for Wings of Arbitrary Plan Form at Subsonic Speeds. NACA Rep. 1056, 1951. (Supersedes NACA TN 2140.)

12. Piland, Robert O.: Summary of the Theoretical Lift, Damping-in-Roll, and Center-of-Pressure Characteristics of Various Wing Plan Forms at Supersonic Speeds. NACA TN 1977, 1949.

13. Sleeman, William C., Jr.: Experimental Investigation at High Subsonic Speeds To Determine the Rolling-Stability Derivatives of Three Wing-Fuselage Configurations. NACA RM L54H11, 1954.

14. Bland, William M., Jr., and Sandahl, Carl A.: A Technique Utilizing Rocket-Propelled Test Vehicles for the Measurement of the Damping in Roll of Sting-Mounted Models and Some Initial Results for Delta and Unswept Tapered Wings. NACA RM L50D24, 1950.

TABLE I

ESTIMATED ACCURACY OF BASIC QUANTITIES

$\left[\text{All increments may be positive or negative}\right]$

Estimated accuracy at a Mach number of -	W, percent	I_Z, percent	I_X, percent	I_{XZ}, percent (1)	M, percent	q, percent	ω, percent	$\left|\dfrac{\dot{\phi}}{\beta}\right|$, percent	$\left|\dfrac{at/g}{\beta}\right|$, percent	$\Omega\dot{\phi}$, deg	α, deg	a, 1/sec
1.07	0.7	2.0	4.0	10.6	1.0	2.3	2.5	3.0	2.0	3	$\frac{1}{2}$	0.1
.89	.7	2.0	4.0	10.6	1.7	3.5	2.5	3.0	2.0	3	$\frac{1}{2}$	.1
.62	.7	2.0	4.0	10.6	4.8	9.7	5.0	3.0	2.0	3	$\frac{1}{2}$	.1

[1]Primarily due to estimated accuracy of principal axis inclination $\left(\frac{1}{2}^\circ\right)$.

TABLE II

CALCULATED ACCURACY OF DERIVATIVES FROM VECTOR ANALYSIS

[All increments may be positive or negative]

Calculated increment due to probable error in -	Accuracy of C_{Y_β} for Mach numbers of -			Accuracy of C_{n_β} for Mach numbers of -			Accuracy of C_{l_β} for Mach numbers of -			Accuracy of C_{l_p} for Mach numbers of -			Accuracy of $C_{n_r} - C_{n_{\dot\beta}}$ for Mach numbers of -		
	1.07	.89	.62	1.07	.89	.62	1.07	.89	.62	1.07	.89	.62	1.07	.89	.62
W	0.006	0.006	0.005	0.001ᵃ	0.001ᵃ	0.002ᵃ	0	0	0	0.001ᵃ	0.002ᵃ	0.005ᵃ	0.06ᵃ	0.06ᵃ	0.15ᵃ
I_Z	------	------	------	0.004	0.005	0.003	-------	-------	--------	-------	-------	--------	0.01	0.02	0.01
I_X	------	------	------	------	------	--------	0.0035	0.0019	0.0018	0.019	0.014	0.014	------	------	------
I_{XZ}	------	------	-------	0.001	0	0	0.0015	0.0019	0.0015	0.007	0.008	0.018	0.24	0.11	0.13
M and q	0.021	0.032	0.081	0.005	0.010	0.020	0.0023	0.0023	0.0056	0.007	0.008	0.018	0.03	0.04	0.08
ω	------	------	------	0.011	0.012	0.019	0.0029	0.0021	0.0035	0.011	0.008	0.016	0	0	0.01
$\left|\dfrac{\dot\phi}{\beta}\right|$	------	------	-------	0.002	0.001	0.001	0.0026	0.0014	0.0013	0	0.001	0.001	0.09	0.03	0.03
$\left|\dfrac{at/g}{\beta}\right|$	0.018	0.018	0.017	0	0	0	0	0	0	0	0	0	0.01	0.01	0.01
$\Omega\dot\phi$	------	------	-------	0.003	0.001	0.001	0.0040	0.0014	0.0014	0.046	0.039	0.038	0.08	0.09	0.11
α	------	------	-------	0	0	0	0.0004	0.0001	0.0001	0.005	0.003	0.003	0.24	0.10	0.13
a	------	------	-------	0	0	0	0.0002	0.0001	0.0002	0.005	0.008	0.013	0.11	0.14	0.24
Probable errors, $\sqrt{\Sigma(\text{increments})^2}$	0.028	0.037	0.083	0.013	0.016	0.028	0.0071	0.0046	0.0073	0.052	0.044	0.049	0.38	0.24	0.37
Probable errors, percent	3.1	4.0	10.0	5.8	5.7	13.1	7.4	7.3	13.2	12.3	14.4	17.0	23.9	13.9	26.4
Calculated values of derivative	-0.907	-0.916	-0.834	0.236	0.277	0.214	0.0956	0.0633	0.0553	-0.442	-0.305	-0.288	-1.59	-1.73	-1.40
Increment due to 0.1 change in estimated value of C_{l_r} or C_{n_p}	------	------	-------	0.010	0.003	0.004	0.0022	0.0014	0.0013	0.023	0.042	0.035	0.43	0.24	0.29

ᵃDue to assumption that the weight vector is equal to zero.
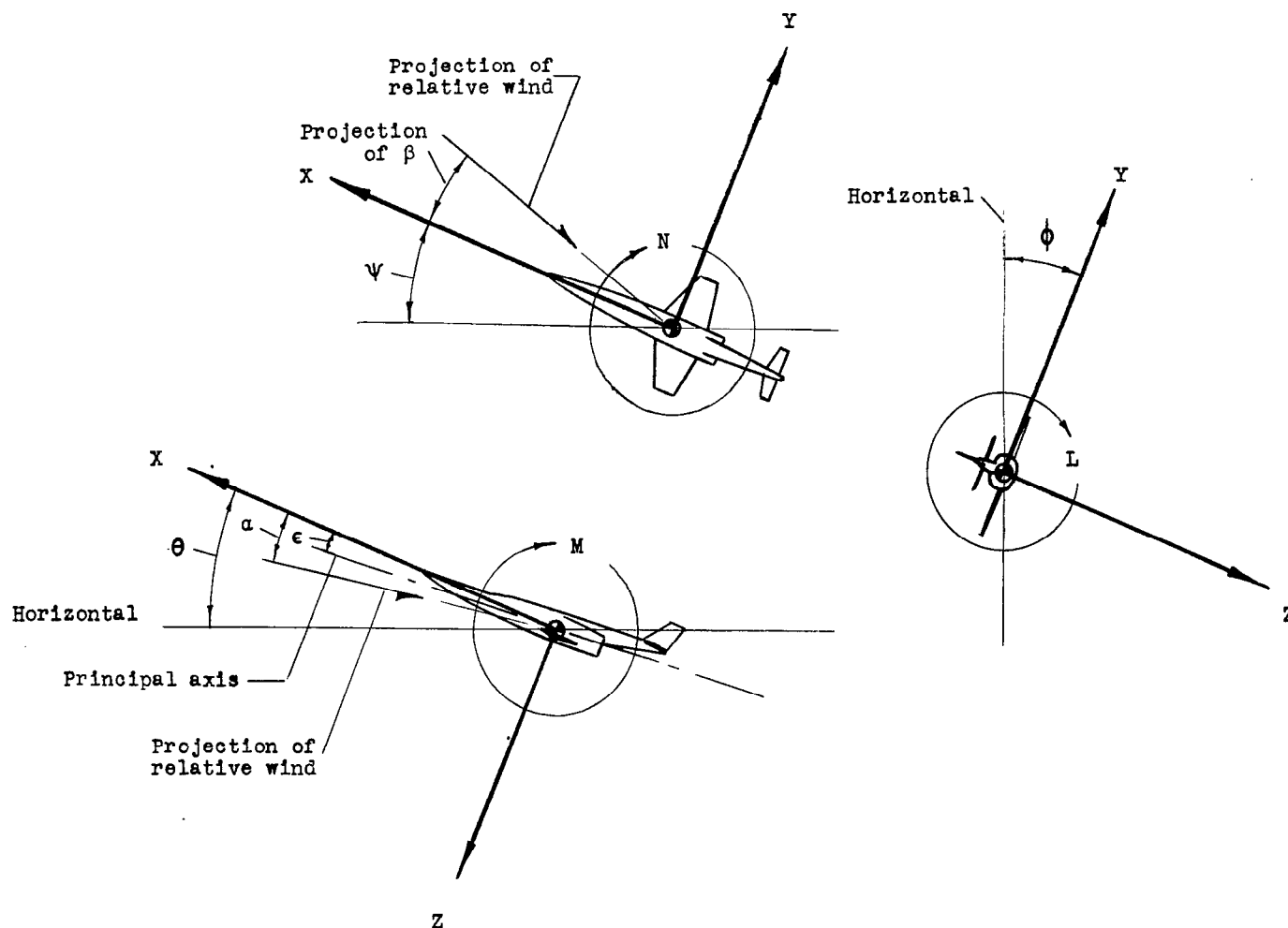
Figure 1.- Sketch depicting the body axes system. Each view represents
a plane of the axes system as viewed along the positive direction of
the third axis. Angular displacements as shown are positive.
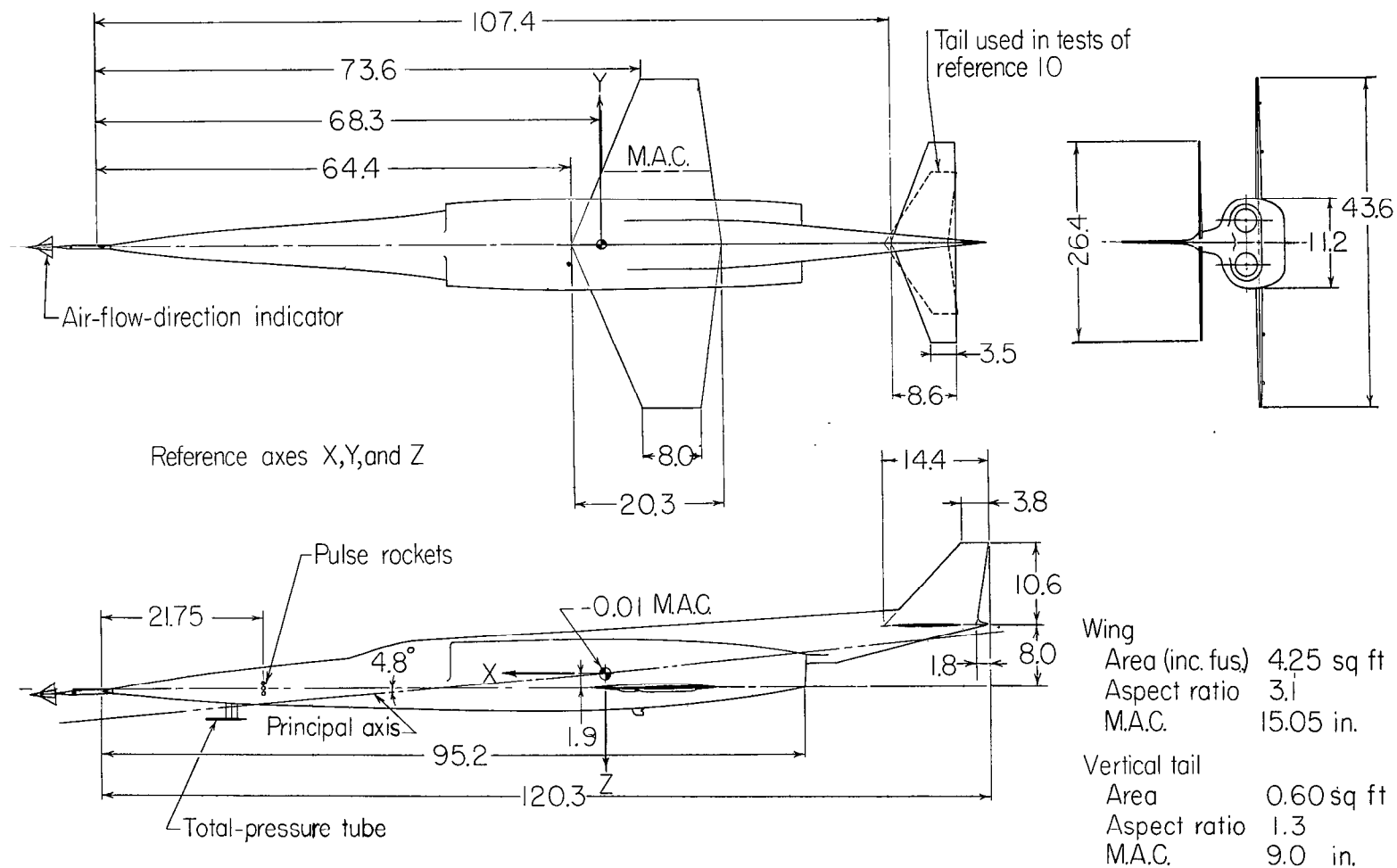
Figure 2.- Sketch of model of Douglas X-3 configuration. All dimensions
are in inches.
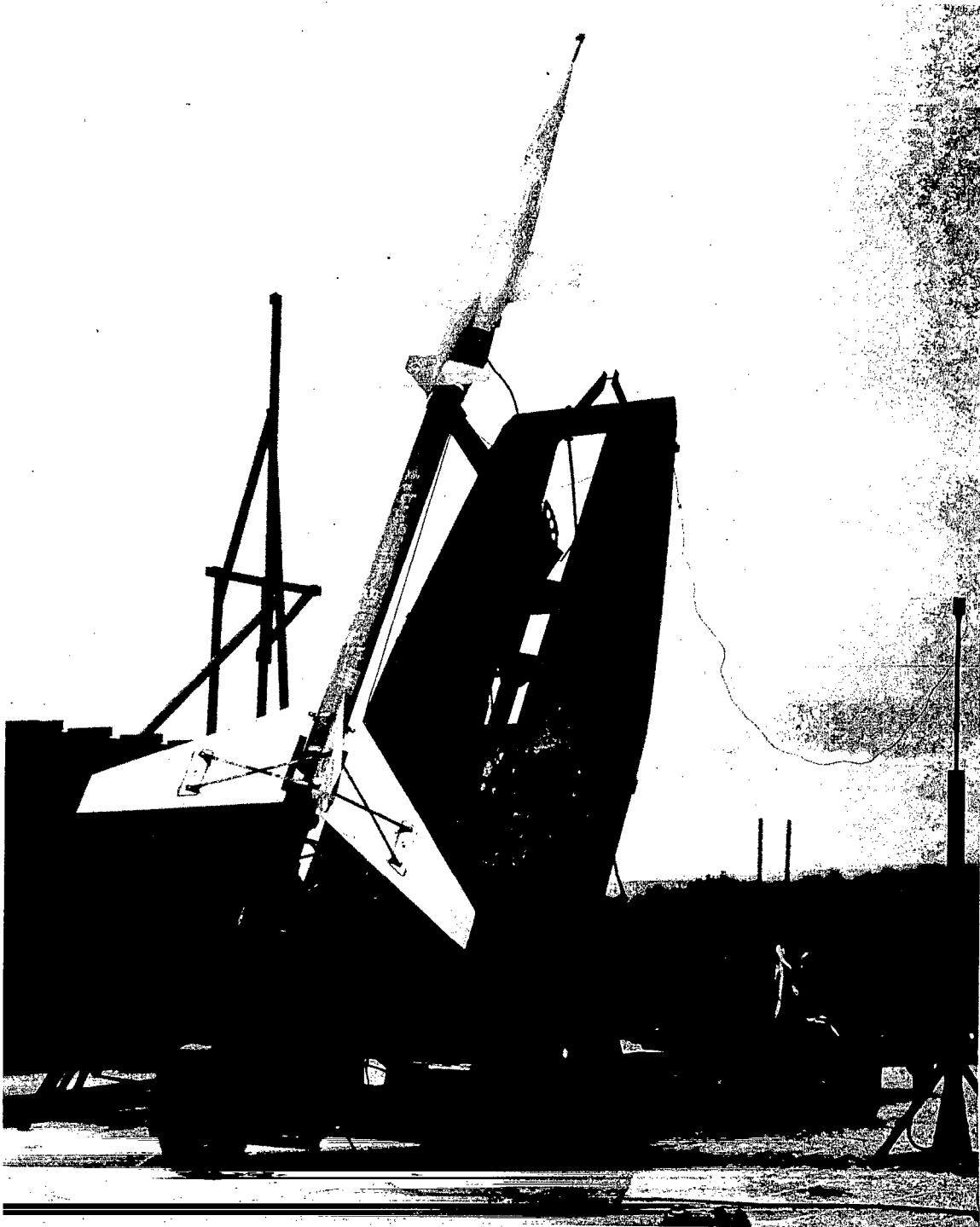
L-82850.1

Figure 3.- Photo of model and booster ready to be launched.
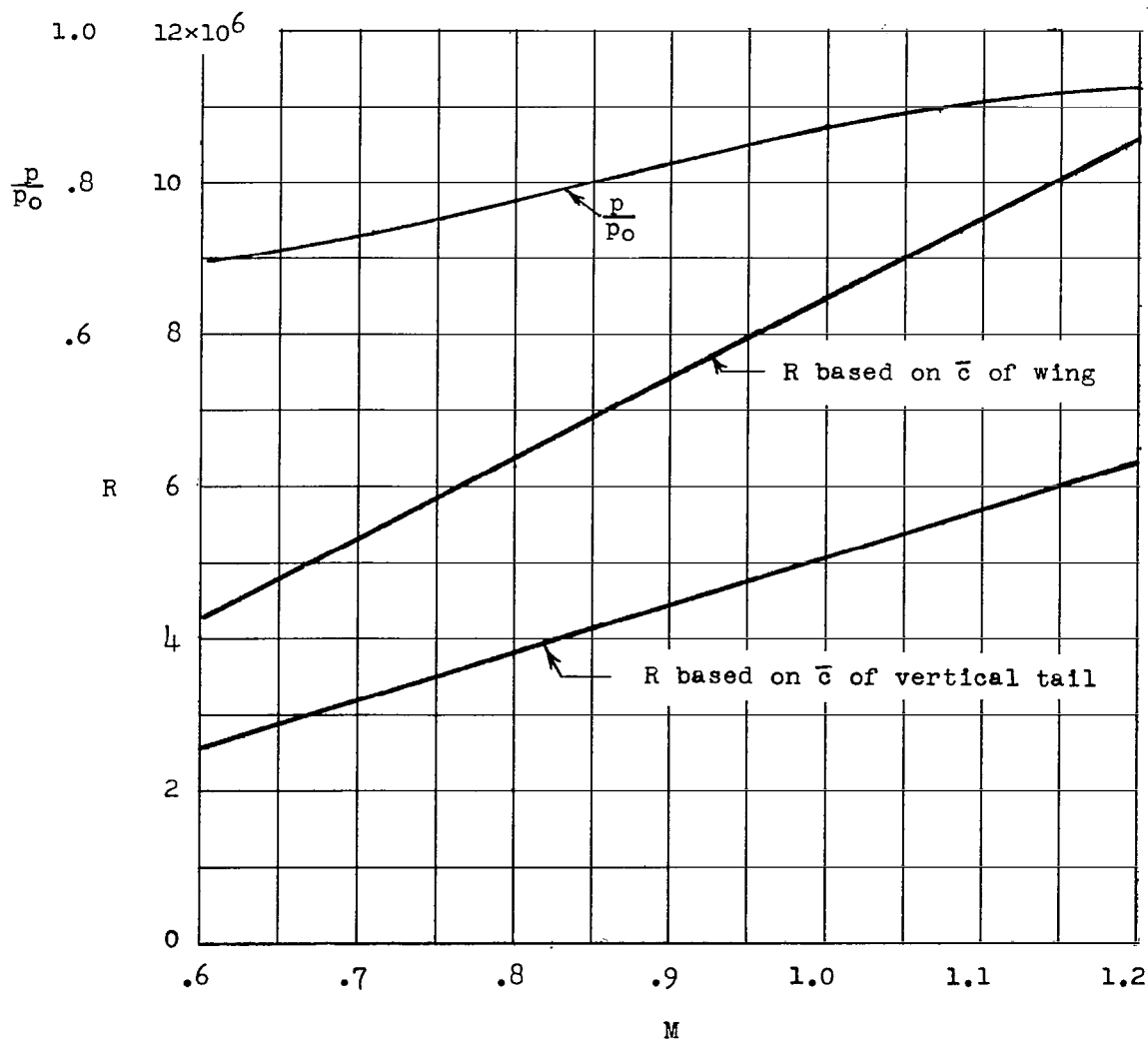
Figure 4.- Variation of static-pressure ratio and Reynolds number with
Mach number.
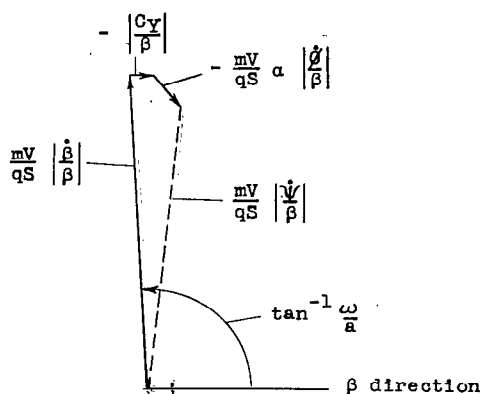
Assume weight vector $= \hat{0}$.

Solve for $\dfrac{\dot{\psi}}{\beta}$ and the direction of $\dot{\psi}$

and for $\dfrac{\ddot{\psi}}{\beta}$ and the direction of $\ddot{\psi}$.

Side-force equation: $\dfrac{mV}{qS}\left|\dfrac{\dot{\beta}}{\beta}\right| + \dfrac{mV}{qS}\left|\dfrac{\dot{\psi}}{\beta}\right| - \dfrac{mV}{qS}\alpha\left|\dfrac{\ddot{\psi}}{\beta}\right| - \left|\dfrac{C_Y}{\beta}\right| = 0$
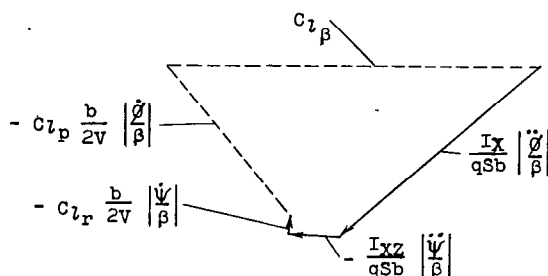
Assume value for C_{l_r}.

Solve for C_{l_p} and C_{l_β}.

Rolling-moment equation: $\dfrac{I_X}{qSb}\left|\dfrac{\ddot{\phi}}{\beta}\right| - \dfrac{I_{XZ}}{qSb}\left|\dfrac{\ddot{\psi}}{\beta}\right| - C_{l_r}\dfrac{b}{2V}\left|\dfrac{\dot{\psi}}{\beta}\right| - C_{l_p}\dfrac{b}{2V}\left|\dfrac{\dot{\phi}}{\beta}\right| - C_{l_\beta} = 0$
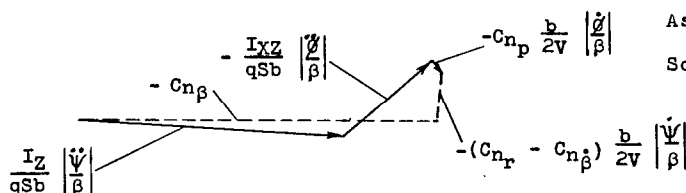
Assume value for C_{n_p}

Solve for $\left(C_{n_r} - C_{n_{\dot{\beta}}}\right)$ and C_{n_β}.

Yawing-moment equation: $\dfrac{I_Z}{qSb}\left|\dfrac{\ddot{\psi}}{\beta}\right| - \dfrac{I_{XZ}}{qSb}\left|\dfrac{\ddot{\phi}}{\beta}\right| - C_{n_p}\dfrac{b}{2V}\left|\dfrac{\dot{\phi}}{\beta}\right| - \left(C_{n_r} - C_{n_{\dot{\beta}}}\right)\dfrac{b}{2V}\left|\dfrac{\dot{\psi}}{\beta}\right| - C_{n_\beta} = 0$

Figure 5.- Typical vector solution of the simplified equations of motion.
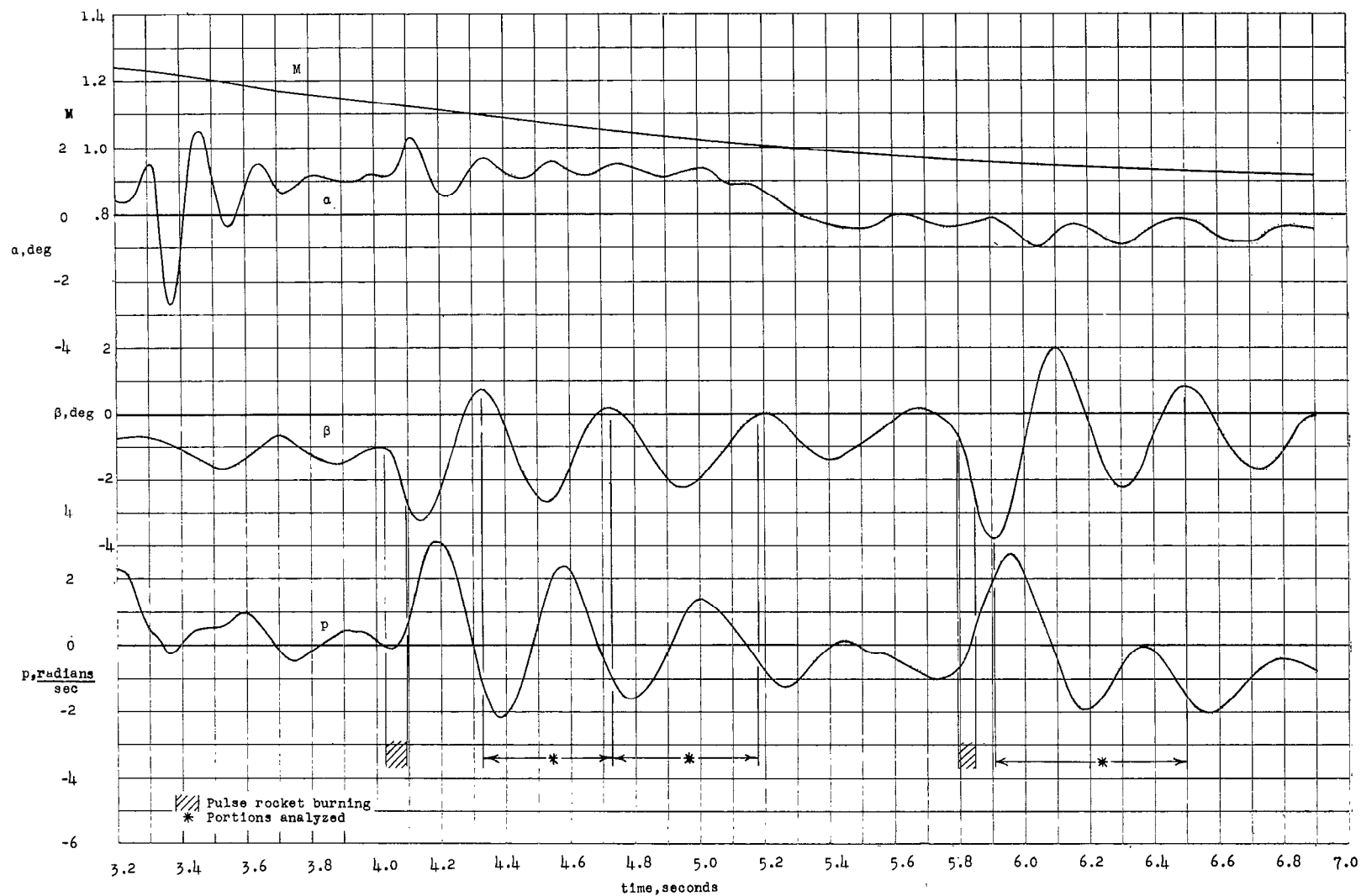
Figure 6.- Flight time histories of angle of attack, angle of sideslip,
rate of roll, and Mach number.
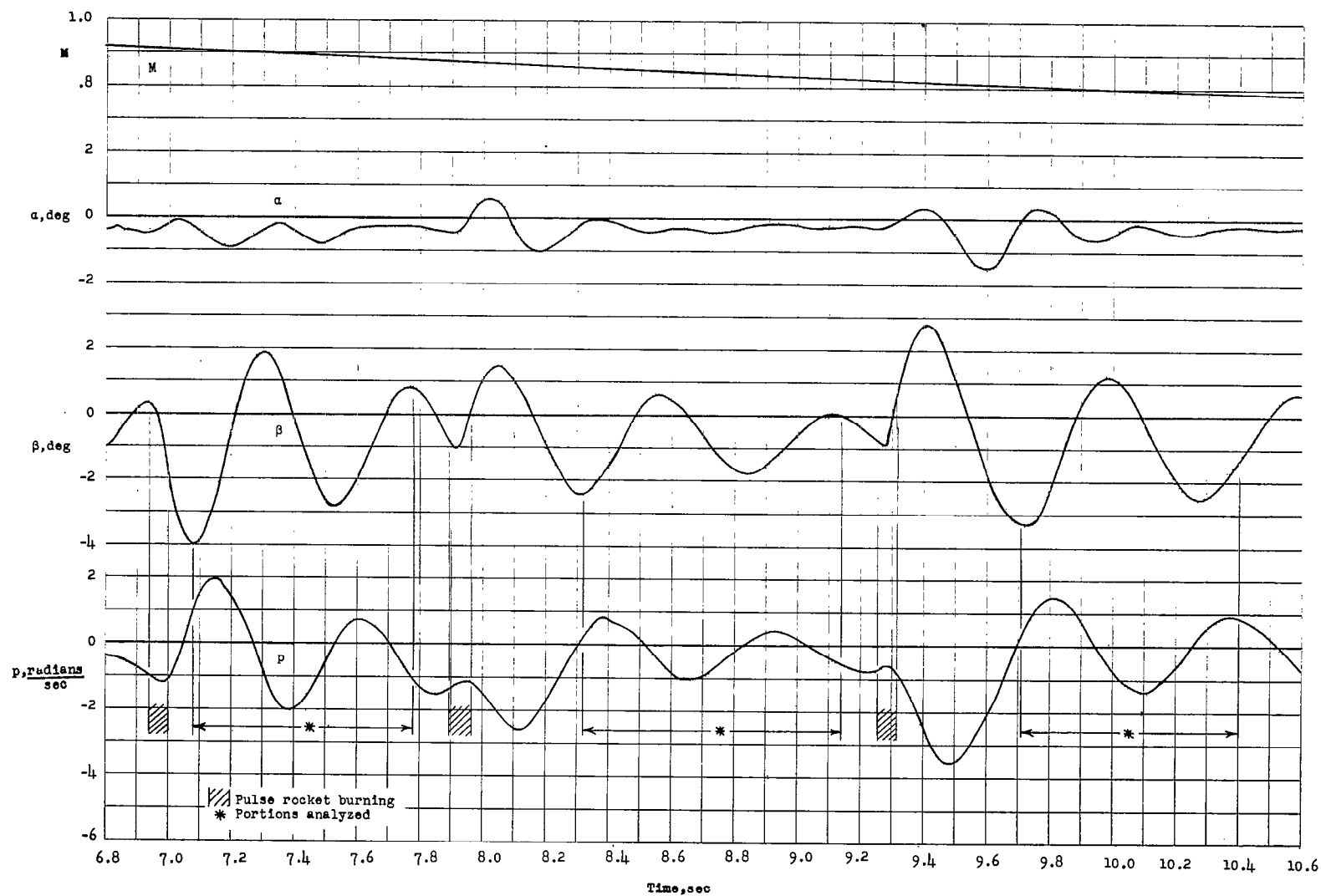
Figure 6.- Continued.
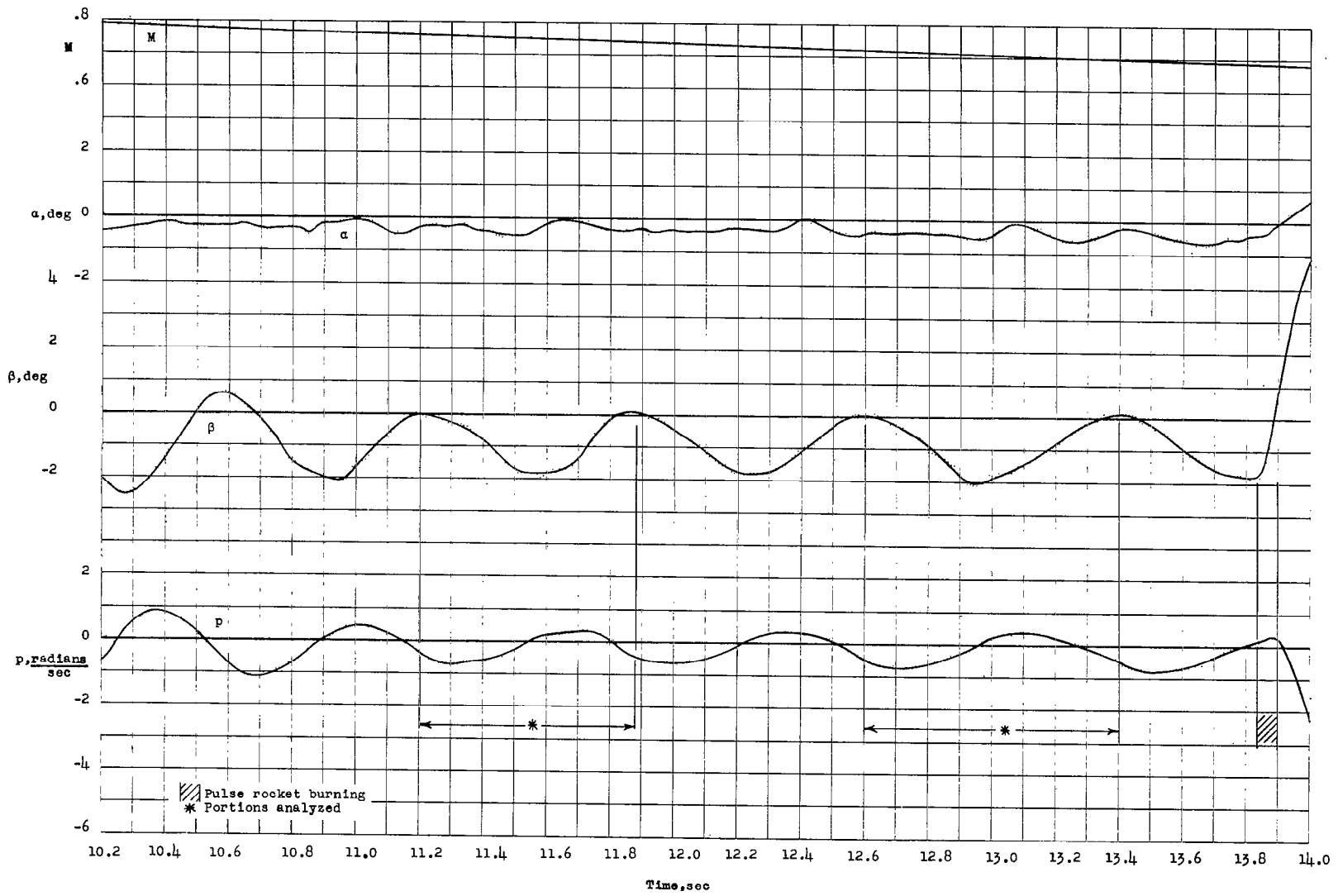
Figure 6.- Continued.
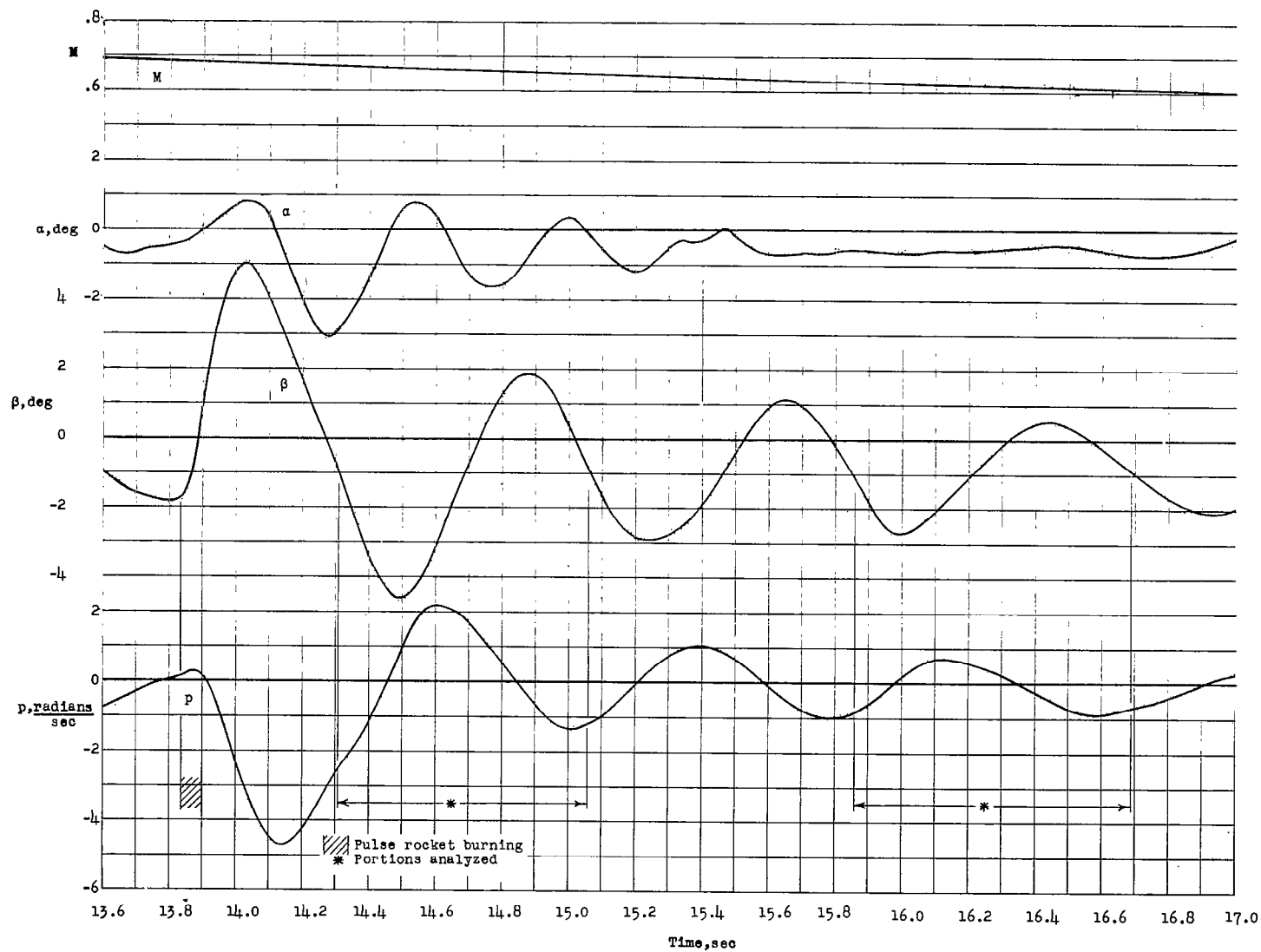
Figure 6.- Concluded.

CONFIDENTIAL NACA RM L54L20
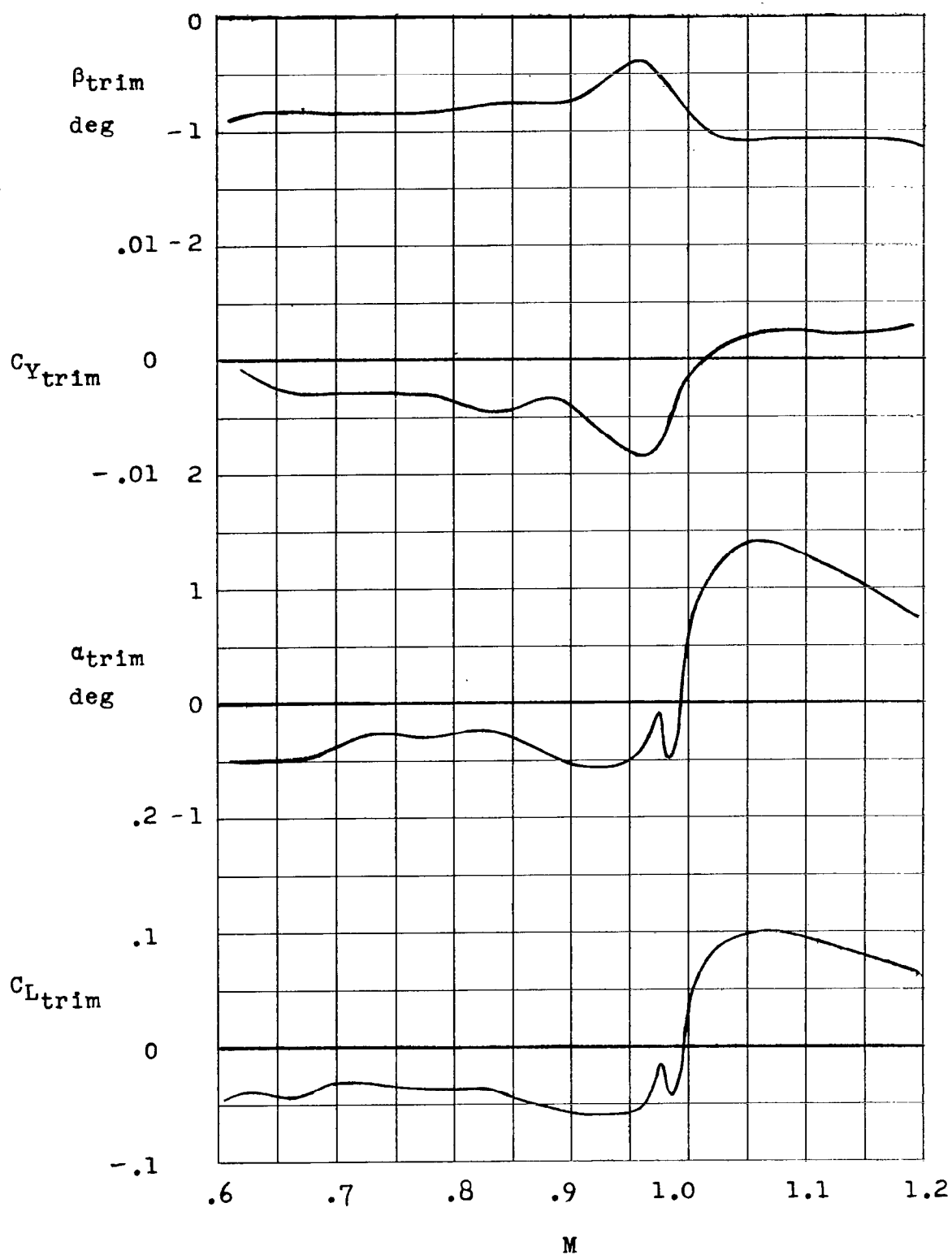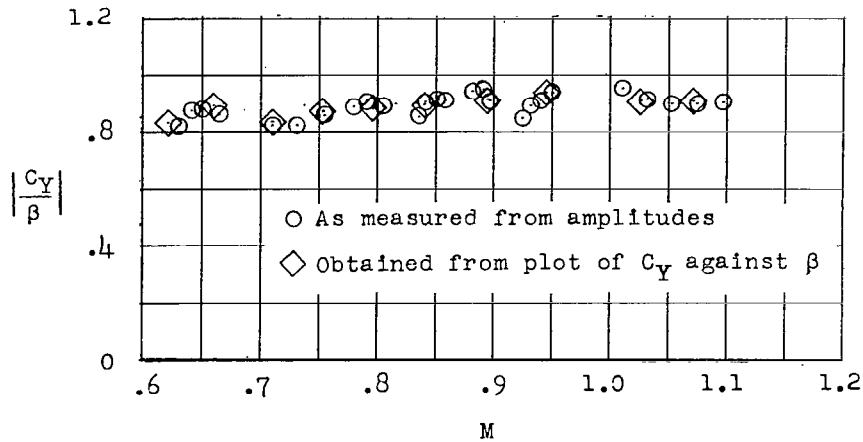
Figure 7.- Trim characteristics of model.
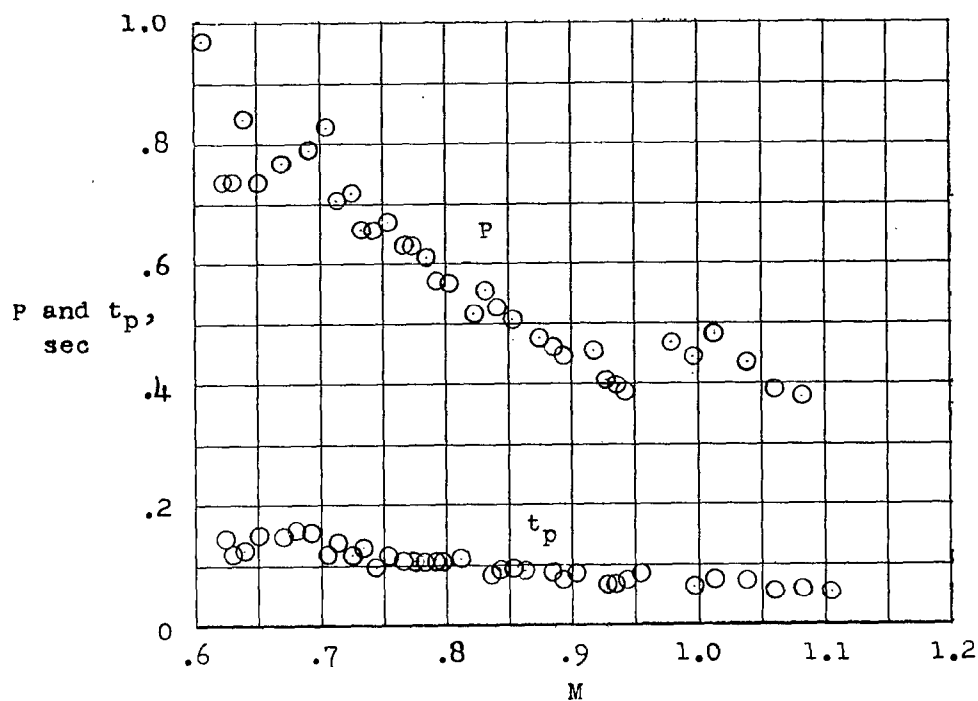
(a) Period of lateral motion and time lag between rate of roll and angle of sideslip.
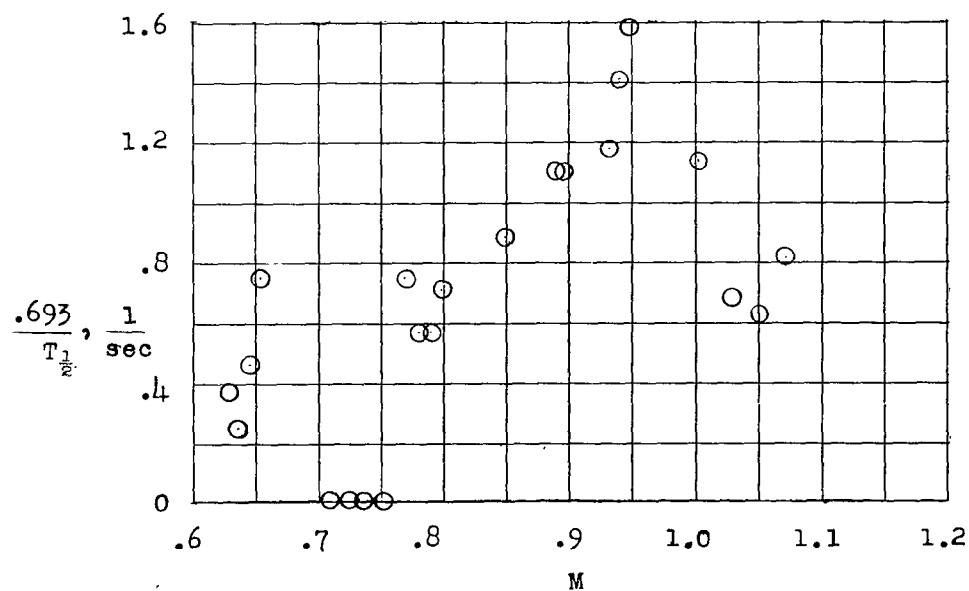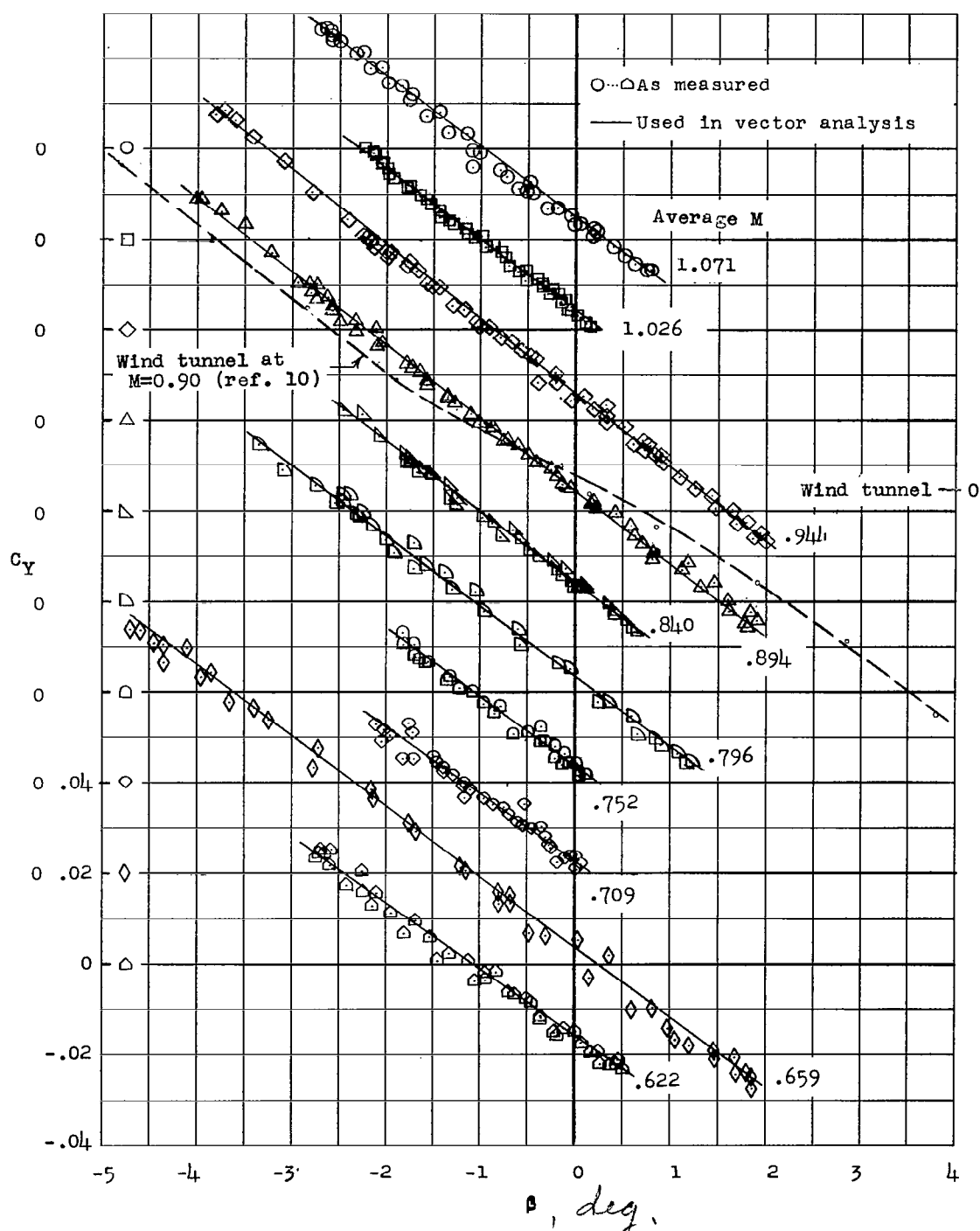

(b) Damping factor.

Figure 8.- General characteristics of lateral oscillation.
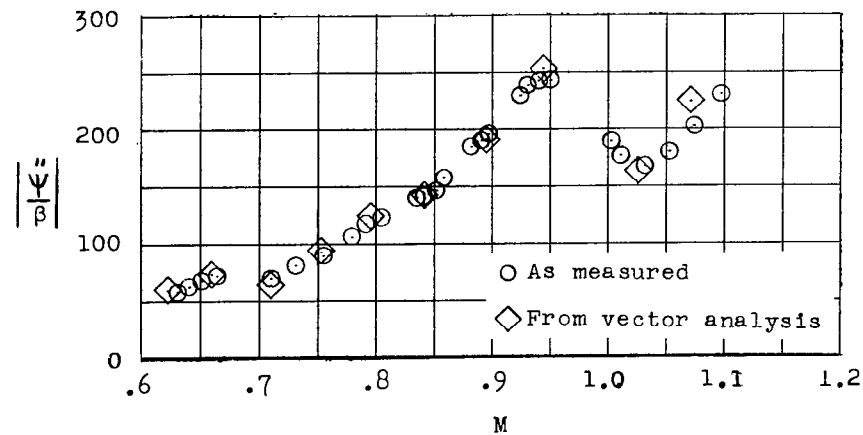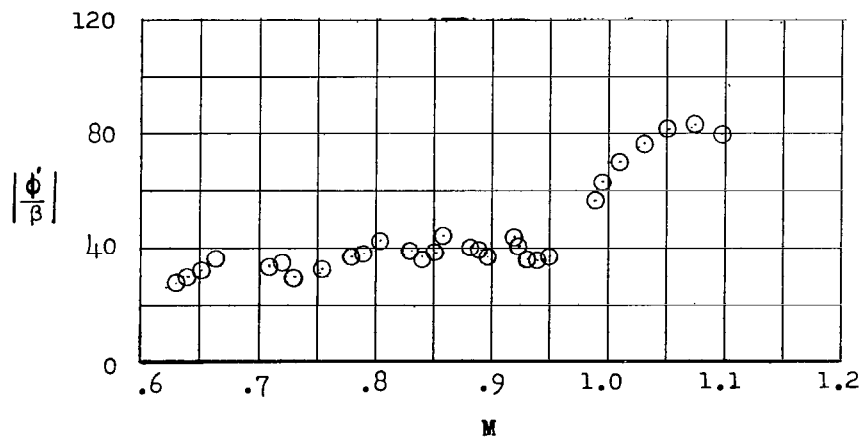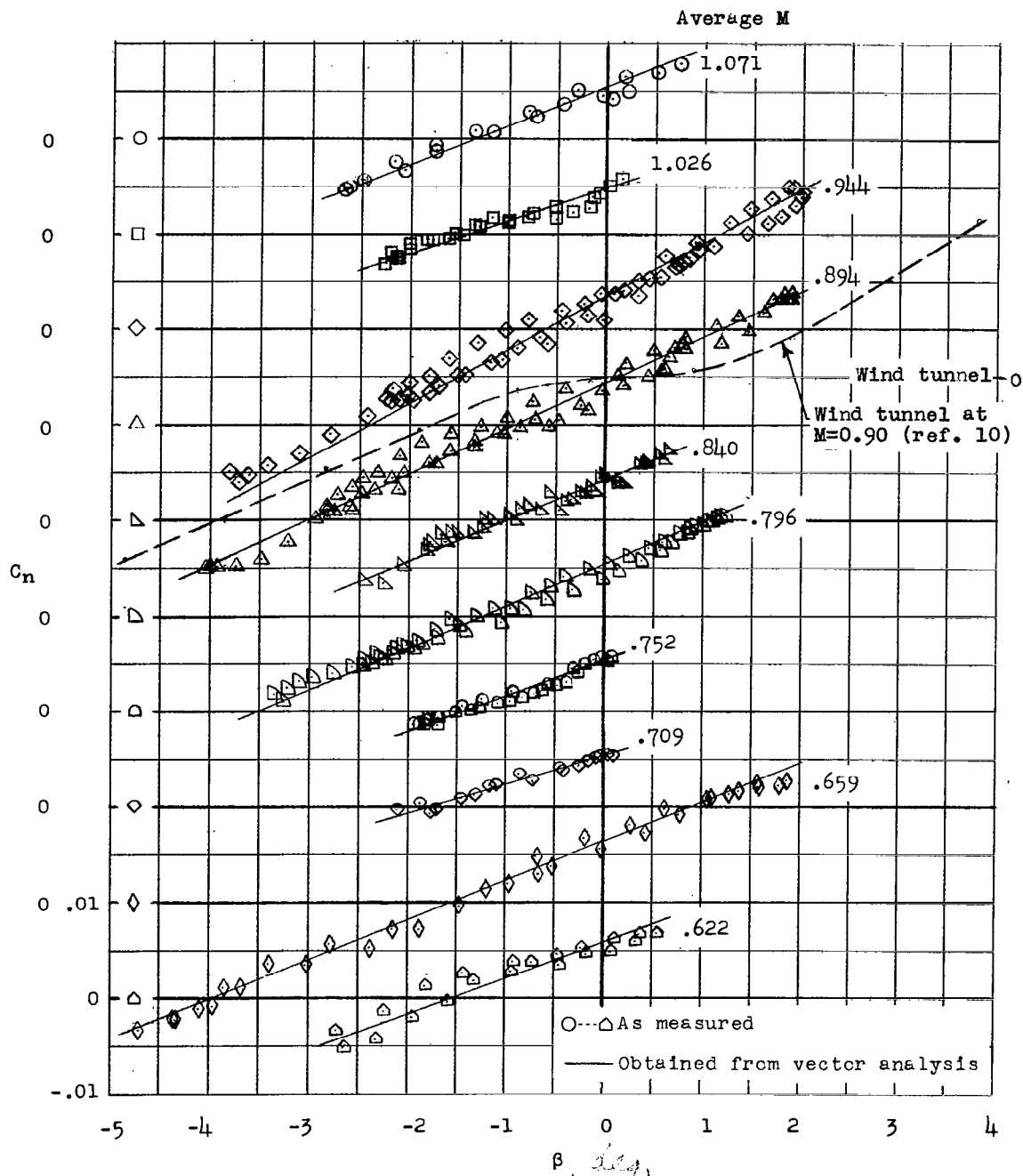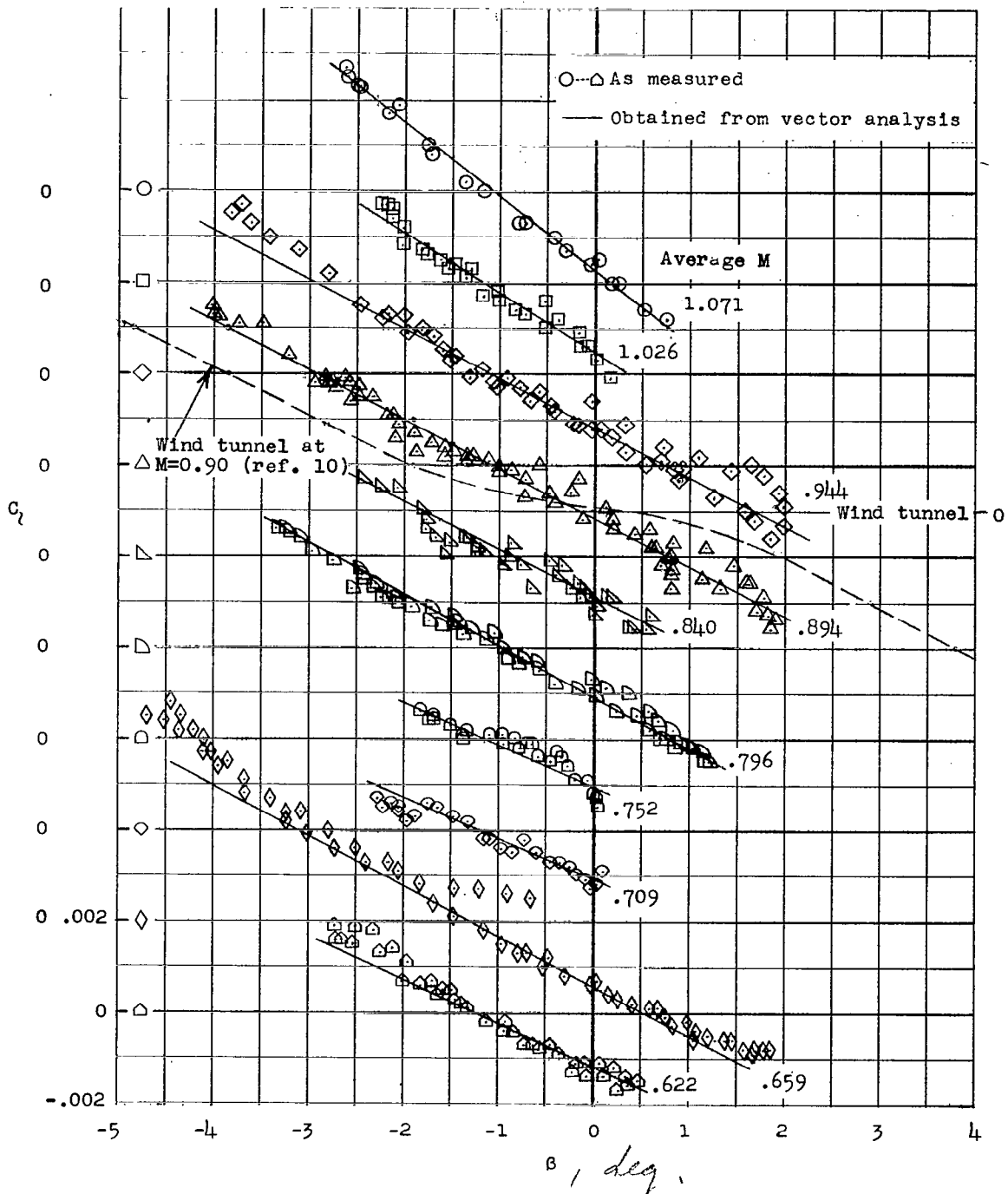
(c) Amplitude ratios.

Figure 8.- Concluded.

(a) Lateral force.

Figure 9.- Variation of lateral force, yawing moment, and rolling moment
with angle of sideslip and Mach number.

(b) Yawing moment.

Figure 9.- Continued.

(c) Rolling moment.

Figure 9.- Concluded.
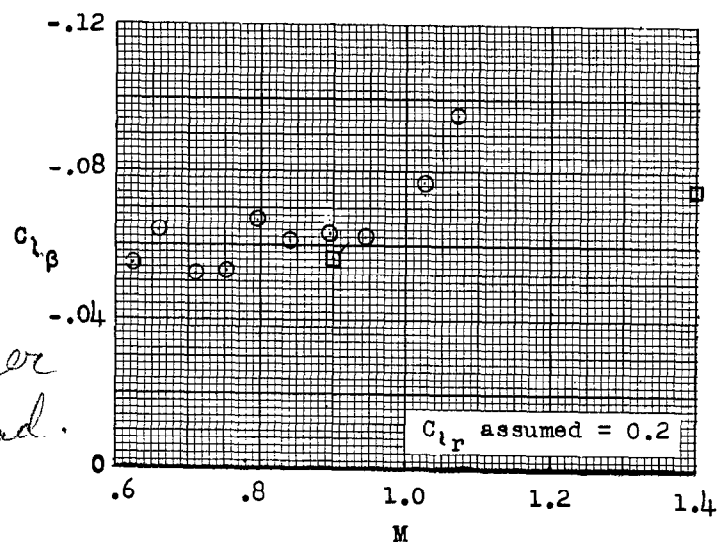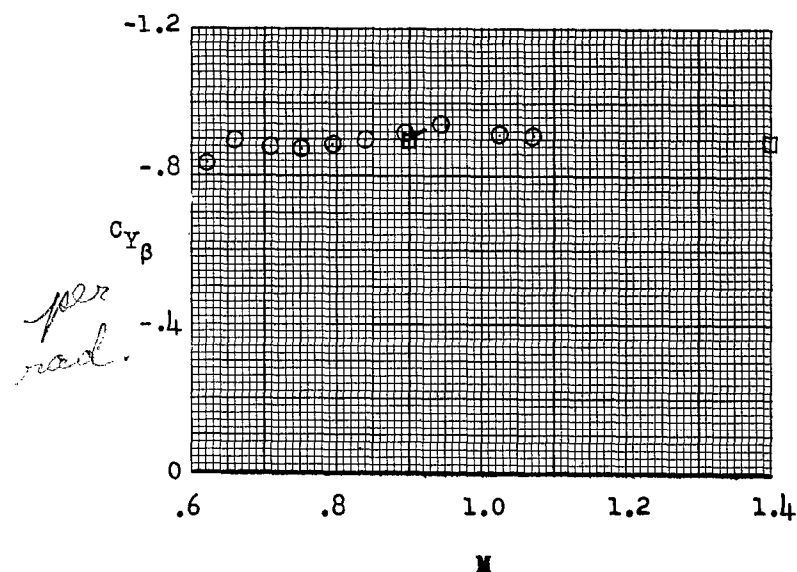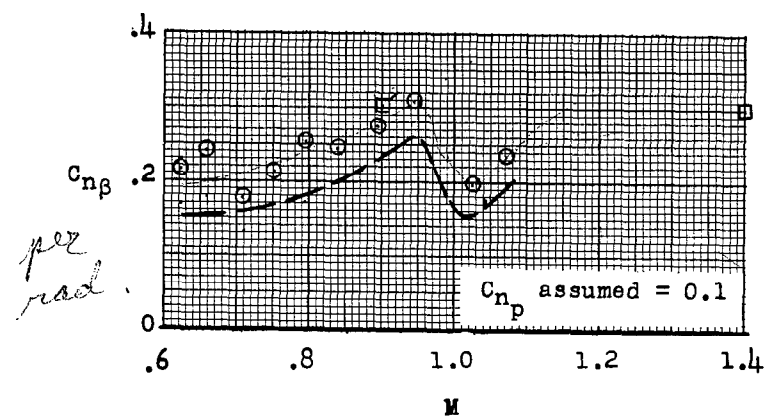
Figure 10.- Variation of static derivatives C_{Y_β}, C_{n_β}, and C_{l_β} with
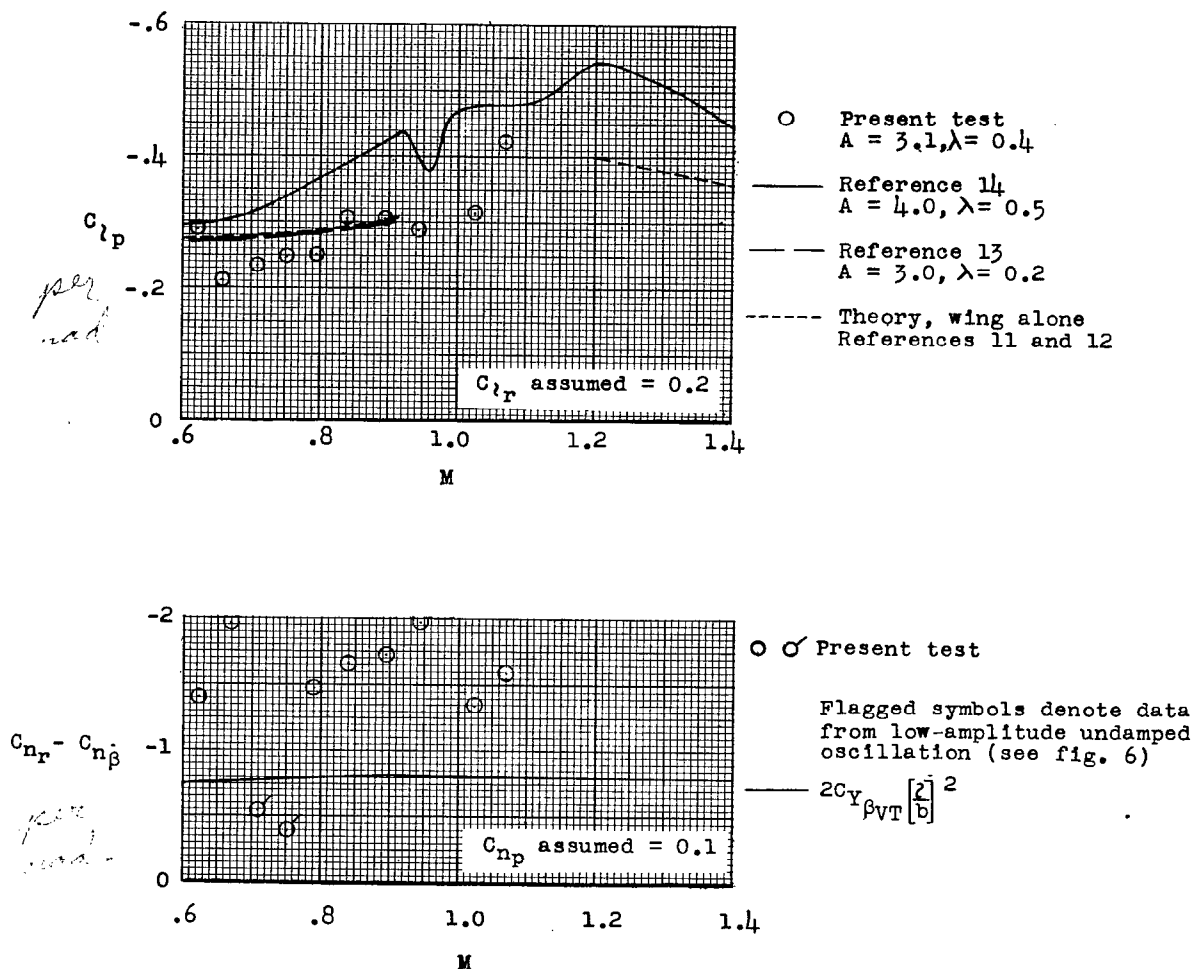
Mach number.

Figure 11.- Damping derivatives C_{l_p} and $C_{n_r} - C_{n_{\dot{\beta}}}$ as obtained from vector analysis.

C̶O̶N̶F̶I̶D̶E̶N̶T̶I̶A̶L̶